Bulk electronic structure of AlB_2-type erbium disilicide with and without Si vacancies

L. Stauffer, C. Pirri, P. Wetzel, A. Mharchi, P. Paki, D. Bolmont, and G. Gewinner
Laboratoire de Physique et de Spectroscopie Electronique, Faculté des Sciences et Techniques, 4 rue des Frères Lumière, 68093 Mulhouse CEDEX, France

C. Minot
Laboratoire de Chimie Organique Théorique, Université Pierre et Marie Curie, 4 place Jussieu, 75230 Paris CEDEX, France

(Received 13 April 1992; revised manuscript received 27 July 1992)

The bulk electronic structure of AlB_2-type Er disilicide is investigated by means of extended Hückel band calculations. The formation of the silicide bands is discussed for both stoichiometric $ErSi_2$ and experimentally observed nonstoichiometric $ErSi_{1.7}$ exhibiting an ordered array of Si vacancies. For both cases, the bands near the Fermi level show a dominant Er $5d$ character. Mixed Er $5d$–Si $3p$ bonding states are located in the 2–4-eV binding energy (BE) range whereas lower-lying bands are composed of almost pure Si $3s,3p$ orbitals. The presence of the Si vacancies significantly affects all the bands and produces two additional bands in the gap observed for stoichiometric $ErSi_2$ along ΓA in the 1.1–2.6-eV BE range. These theoretical results are compared to photoemission data collected at normal emission from $ErSi_{1.7}$ films grown epitaxially on Si(111). The agreement is surprisingly good when the emission from surface states is taken into account. In particular, the experiments indicate a Si vacancy-induced band located near 1.2 eV BE as well as the band folding resulting from the specific ordered arrangement of the Si vacancies (period doubling along c) as assumed in the calculations.

I. INTRODUCTION

Many studies of the rare-earth (RE) silicides have already been made because of their fundamental and technological interest. Knapp and Picraux have first demonstrated that numerous RE silicides can be grown epitaxially on Si(111) with a hexagonal $RESi_{1.7}$ structure.[1,2] This structure consists of a hexagonal phase based on the AlB_2 structure but with 15–20% vacancies on the Si sublattice. Among these silicides, $ErSi_{1.7}$ seems to be a good candidate for technological applications such as epitaxially grown semiconductor-metal-semiconductor heterostructures, since it has a relatively small lattice mismatch to Si(111) ($\sim -1.22\%$) and an electrical resistivity comparable to that of $CoSi_2$ or $NiSi_2$.[2,4] $ErSi_{1.7}$ grows epitaxially on Si(111) by solid phase epitaxy,[3–6] by coevaporation of the Er and Si species on Si(111),[3,4] and by ion-beam synthesis.[7] In epitaxially grown $ErSi_{1.7}$ films, the Si vacancies are periodically distributed over the silicide film giving rise to electron-diffraction superstructures, as it is observed for $YSi_{1.7}$,[8,9] $TbSi_{1.7}$,[10] $YbSi_{1.7}$,[11] and $GdSi_{1.7}$ (Ref. 12) thin films. Its formation has been investigated by several groups using photoemission experiments.[6,13–15] All these experiments have pointed out that the valence-band spectra recorded on $ErSi_{1.7}$ are dominated by numerous features, involving both corelike Er $4f$ and mixed Er $5d$–Si $3s3p$ states, whose origin is poorly understood. A clear understanding of the $ErSi_{1.7}$ (and also other $RESi_{1.7}$ silicides) needs a good description of the bulk electronic structure, via a band-structure calculation, for instance, which takes into account the presence of ordered Si vacancies within the silicide.

The aim of this paper is to present the results of a theoretical study of the band structure of bulk $ErSi_2$ and $ErSi_{1.7}$ silicides and a comparison with experimental data. We adopt the crystalline extension of the extended Hückel theory.

The paper is organized as follows. In Sec. II we recall briefly the theoretical method and present the band-structure calculations performed on $ErSi_2$ and $ErSi_{1.7}$. A comparison with available experimental data is presented in Sec. III, and we draw conclusions in the last section.

II. THEORETICAL RESULTS

The calculations have been performed using the crystalline extension of the extended Hückel method (EHT). In the EHT scheme,[16,17] the periodic system is defined by a set of valence orbitals contained in a unit cell and by three translation vectors. These atomic orbitals are described by Slater wave functions. Slater exponents and atomic energy levels are reported in Table I. Then one can form a set of Bloch sums. The crystal orbitals are linear combination of the Bloch sums. The variational theorem leads to a generation of the secular determinant $|H_{\mu\gamma}(k)-e(k)S_{\mu\gamma}(k)|$, where the interaction elements, $H_{\mu\gamma}(k)$ and the overlap integrals $S_{\mu\gamma}(k)$ are defined in terms of Bloch sums. $e(k)$ is the energy associated with the orbital for a given k point. In the EHT theory, the $H_{\mu\gamma}(k)$ are derived from the $S_{\mu\gamma}(k)$ terms and from the atomic energy levels $H_{\mu\mu}$ and $H_{\gamma\gamma}$ using the weighted formula which replaces the 1.75 parameter of the Wolfsberg-Helmoltz formula by an expression depending on the difference between the atomic energy levels.[18] To calculate the band structure for selected values of k in the

TABLE I. Extended Hückel parameters [matrix elements H_{ii} (eV) and Slater exponents for Si and Er].

Orbital	H_{ii} (eV)	Slater exponent
Er 6*s*	−4.882	1.396
Er 6*p*	−4.882	1.396
Er 5*d*	−6.917	2.199
Si 3*s*	−17.30	1.45
Si 3*p*	−9.2	1.45

irreducible part of the Brillouin zone (BZ), we assume that the Er configuration of $5d^1 6s^2 4f^{11}$ and ignore the corelike *f* electrons. The Fermi level E_F is obtained from a calculation using a set of representative *k* points (uniform grid) in the irreducible part of the BZ affected by an appropriate weighting factor.

The hexagonal Er silicide crystallizes in the AlB_2 structure as depicted in Fig. 1. This structure consists of alternating (0001) planes made of either Er or Si arranged, respectively, in a hexagonal lattice and in a honeycomb array. The periodic *c* along the [0001] axis is the distance between Er or Si planes. Experimentally, this ideal structure of Er silicide is not observed in epitaxial growth on Si(111), but a nonstoichiometric form $ErSi_{1.7}$ which contains an ordered array of Si vacancies is observed instead.[2,3] We assume the same ordered superstructure as has been revealed in the case of Y silicide grown on Si(111):[9] in a given Si(0001) plane one atom out of six is missing. The next Si plane just below or just above has the same structure but is rotated by 120° around [0001]. Thus only every second Si plane has the same orientation and the period along [0001] is 2*c*. The Si vacancies give a $\sqrt{3}\times\sqrt{3}R30°$ superstructure mesh in a Si(0001) plane which is observed on epitaxial layers by low-energy electron diffraction (LEED).

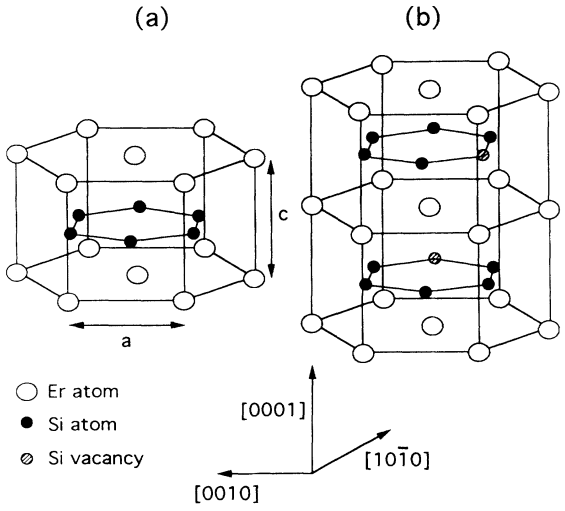

FIG. 1. (a) $ErSi_2$, and (b) $ErSi_{1.7}$ unit-cell perspective views. Open circles denote Er atoms, black circles Si atoms, and striped circles Si vacancies. $c = 4.09$ Å; $a = 3.84$ Å.

Figure 1 compares the unit cells of $ErSi_2$ and $ErSi_{1.7}$. In order to investigate the influence of the Si vacancies the band calculations are carried out for Er silicide in the AlB_2-type structure either with or without Si vacancies arranged as described above. We assume that the relaxation of the Si atoms around the vacancies is negligible. To make the comparison more lucid, the results are presented in both cases in the reduced BZ corresponding to the superstructure unit cell of $ErSi_{1.7}$, namely $\sqrt{3}\times\sqrt{3}R30°$ in the (0001) plane and 2*c* along the [0001] axis. The superstructure unit cell contains an atomic basis made of either six Er and twelve Si in the case of $ErSi_2$ or six Er and ten Si in the case of $ErSi_{1.7}$. For comparison with the experimental results, the calculations mainly concentrate on the ΓA symmetry direction of the reduced BZ.

A. The $ErSi_2$ band structure

Figure 2 presents the band dispersion of the $ErSi_2$ structure along the ΓA direction of the reduced BZ. Energies are referred to the Fermi level E_F. Three different energy regions can be distinguished in the band structure:

(i) The region close to the Fermi level E_F, where we find bands [(9)–(14)] arising essentially from Er 5*d* levels.

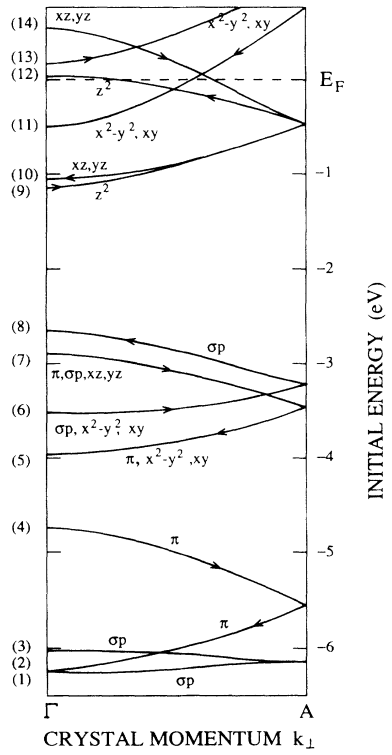

FIG. 2. Band dispersion of the $ErSi_2$ structure. These results are presented in the reduced BZ corresponding to the structure unit cell of $ErSi_{1.7}$, namely $\sqrt{3}\times\sqrt{3}\ R30°$ in the (0001) and 2*c* along the [0001] axis. The arrows indicate the direction of the folding. Only the main components of the wave functions are reported on the figure. s,σ_p (or p_x,p_y) and π (or p_z) refer to the Si orbitals and x^2-y^2,*xy*,z^2,*xz*,*yz* to the Er 5*d* orbitals.

(ii) The region between -2.6 and -4.0 eV, containing the bands induced by bonding interaction between Si $3p$ states and Er $5d$ states. The twofold degenerated bands (6) and (8) arise mainly from the mixing of Si σ_p (or Si p_x and Si p_y) levels with Er d levels, while the fourfold degenerated bands (5) and (7) result from the interaction of the nonbonding Si π (or Si p_z) levels with the Er d levels.

(iii) The region between -4.7 and -6.2 eV, where the bands are originating from almost pure Si $3p$ orbitals. Bands (2) and (4) are pure Si π bands whereas the twofold degenerated bands (1) and (3) essentially derive from Si σ_p orbitals. More details on the bands character are given on the relevant figure.

Finally, we note the existence of a gap of about 1.5 eV between the lowest Er $5d$ band (9) and the upper Er $5d$–Si $3p$ band (8).

B. The $ErSi_{1.7}$ band structure

Turning to the results for $ErSi_{1.7}$, presented in Fig. 3, we notice that the presence of Si vacancies introduces important modifications in the band structure. We can now distinguish four different energy regions: (i) The bands (12) to (14) originating mostly from the Er $5d$ orbitals are located around the Fermi level E_F; (ii) the region between -0.8 and -1.8 eV contains twofold degenerate bands [(10) and (11)] arising from bonding interactions between Si σ_p states and Er d states; (iii) the mixing between the nonbonding Si-π states and Er d states is found in the -2.0- to -3.2-eV energy range; and (iv) the bands located between -3.7 and -5.0 eV result from nearly pure Si π orbitals [(2) and (5)] or Si σ_p orbitals [(1) and (4)].

Comparing the $ErSi_{1.7}$ band structure with the $ErSi_2$ one, we clearly remark that all the bands are significantly affected by the presence of Si vacancies. Two major changes occur: we first observe a shift of about 1 eV of nearly all the bands toward the Fermi level; second, two additional bands [(10) and (11)] appear in the gap observed for stoichiometric $ErSi_2$. These results may be understood if we consider that, in the presence of a Si vacancy, three hybrid orbitals pointing toward the missing atom are unmatched (Fig. 4). As the crystal orbitals are delocalized, these three hybrids combine. At Γ, they generate one "A" and two "E" combinations, leading to supplementary bands. The labels "A" and "E" are reminiscent of the symmetry group since the c axis passing through the vacancy is a C_3 axis. A detailed analysis of the electronic structure of a honeycomb monolayer of Si atoms with vacancies[19] allows us to point out that the bands (10) and (11) are induced by the "E" vacancies in the $ErSi_{1.7}$ structure.

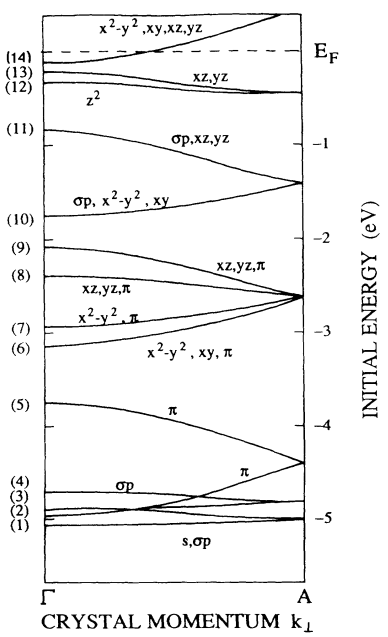

FIG. 3. Band dispersion of the $ErSi_{1.7}$ structure. The notations are those used in Fig. 2.

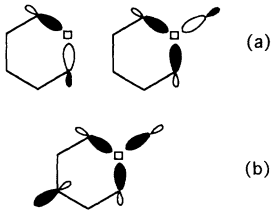

FIG. 4. "A" and "E" vacancies; the presence of vacancy (□) in the (0001) Si graphitelike plane leads to the appearance of three unmatched hybrid orbitals pointing toward the missing atom. Three combinations are so generated: (a) two "E" and (b) one "A". The white and black regions correspond to opposite phases.

III. COMPARISON BETWEEN EXPERIMENTAL AND THEORETICAL RESULTS

Experiments were carried out *in situ* in an ultrahigh vacuum system consisting of a molecular-beam epitaxy chamber and an analysis chamber equipped with LEED and angle-resolved photoemission techniques. Angle-resolved ultraviolet photoemission spectroscopy (ARUPS) measurements were recorded using a gas discharge lamp permitting the valence-band analysis with several photon energies, i.e., He_I ($\hbar\omega=21.2$ eV), He_{II} ($\hbar\omega=40.8$ eV), Ne_I ($\hbar\omega=16.8$ eV), Ne_{II} ($\hbar\omega=26.8$ eV), and Ar_I ($\hbar\omega=11.8$ eV). The photoelectrons were analyzed in normal emission along the [0001] $ErSi_{1.7}$ axis with a hemispherical analyzer whose acceptance angle was set to $\pm 1°$, thus probing k points along the ΓA direction of the $ErSi_{1.7}$ bulk BZ.

A 300-Å-thick $ErSi_{1.7}$ layer is grown onto a clean Si(111) 7×7 wafer in two steps. First a three-monolayers-thick Er film is deposited at room temperature on Si(111) and annealed at $\sim 500\,°C$. An epitaxial $ErSi_{1.7}$ template is then formed as attested by a sharp $\sqrt{3}\times\sqrt{3}$ $R30°$ LEED pattern. Sixty Er monolayers are then deposited onto this template layer maintained at 500 °C. Such a procedure leads to the formation of an ordered $ErSi_{1.7}$ layer. The LEED pattern is $\sqrt{3}\times\sqrt{3}$ $R30°$, although it is superimposed on a diffuse background at this stage of the growth procedure. The advantage of this

procedure is that the Er atoms react with the substrate and this avoids the exposure of pure Er to the residual contaminants. X-ray photoemission spectroscopy (XPS) measurements show a very low degree of contamination of the silicide surface. The $ErSi_{1.7}$ layer is subsequently annealed up to 700–750 °C. The LEED pattern is then $\sqrt{3}\times\sqrt{3}$ $R30°$ with sharp spots and the diffuse background is considerably diminished. A well-ordered epitaxial $ErSi_{1.7}$ is achieved at this stage.

Figure 5 shows angle-resolved spectra recorded on $ErSi_{1.7}$ (0001) at normal emission taken with two photon energies, i.e., $\hbar\omega=21.2$ eV and $\hbar\omega=40.8$ eV. As previously shown, the $ErSi_{1.7}$ spectra involve both Er $4f$ and Er $5d$–Si $3s3p$ states.[6,13–15] In $ErSi_{1.7}$ the Er atoms are in a trivalent Er^{3+} form, giving rise to a Er $4f^{10}$ final-state multiplet located in the 4–11-eV binding energy (BE). As shown in Fig. 5, the Er $4f$-related peaks are more or less visible depending on the photon energy. With the photon energy range used in this experiments, their intensities increase with photon energy and they are only fully developed for $\hbar\omega=40.8$ eV. Thus the Er $5d$–Si $3s3p$-related states can be easily analyzed in the 0–5-eV BE window without interferences with the $4f$ states, whereas their detection in the higher BE region of the spectra is more difficult. That is why we have focused our attention on the low BE side of the $ErSi_{1.7}$ valence band.

Figure 6 displays angle-resolved spectra of the 0–5-eV BE region taken at normal emission with a fixed light incidence angle and five photon energies in the 10–41-eV range. In order to map the $E_i(k)$ dispersion of the initial-state bands along the ΓA direction, we have assumed a direct transition model and we have used a single free-electron final band dispersion.

In this case we can determine the $k_\perp$ component of crystal momentum for a given transition by

$$k_\perp=\left[\frac{2m}{\hbar^2}(\hbar\omega+V_0-\phi-E_i)\right]^{1/2}$$

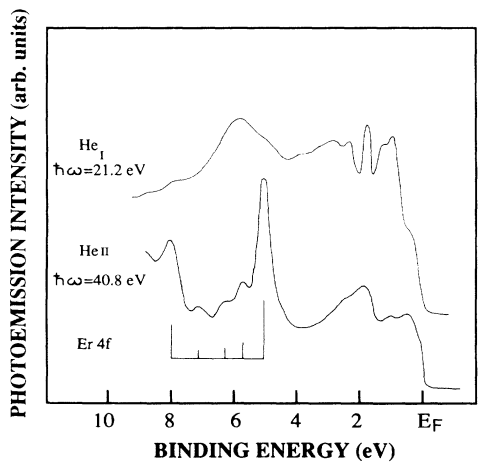

FIG. 5. Normal-emission photoelectron spectra from $ErSi_{1.7}$(0001) taken with He_I and He_{II} radiations. Vertical bars indicate the low-lying BE part of the Er $4f$ final-state multiplet structure.

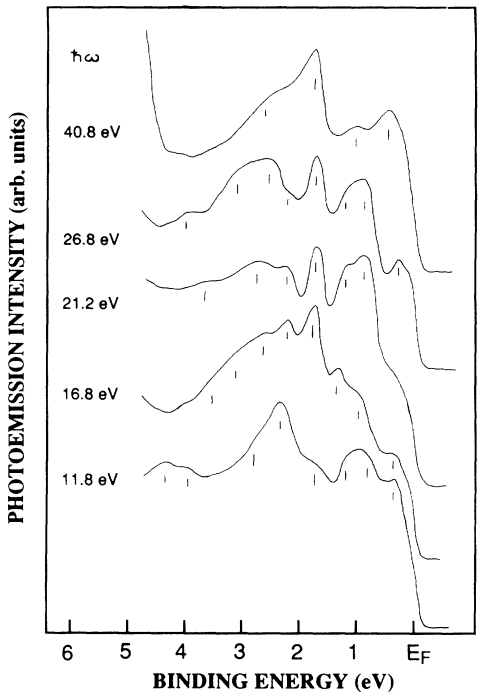

FIG. 6. Normal-emission photoelectron spectra from $ErSi_{1.7}$(0001) taken at various photon energies.

for a polar angle $\Theta=0$ where V_0 is the inner potential, ϕ the sample work function, $\hbar\omega$ the incident photon energy, and E_i the initial electron state energy. The sample work function was found to be $\phi=4.75\pm0.10$ eV and the crystal inner potential was taken to be $V_0=12$ eV.

Figure 7 compares the experimental data along the ΓA direction of the bulk BZ with the theoretical bands (solid lines) described in Sec. II B. Binding energies corresponding to the peaks and features indicated by tics in Fig. 6 are plotted at the $k_\perp$ values determined by the final band. The experiments show essentially eight bands in the 0–5-eV BE range. A remarkably good overall agreement is observed between experimental and theoretical bands for the BE's as well as for the dispersion of the low-lying Si π-derived band (3.7–4.6-eV BE), the Er $d_{x^2-y^2,xy}$–Si π and Er-$d_{x^2-y^2}$–Si π bands (2.6–3.1 eV BE) and the Er d_{z^2}, Er $d_{xz,yz}$ derived bands (0.2–0.6-eV BE). Additionally, Fig. 7 displays a group of levels near point A located at ~0.9, 1.2, 1.8, and 2.2 eV BE, which show a poorer agreement with theoretical bands. Actually none of these levels shows a significant experimental dispersion with photon energy in contrast with the theory. Recent experiments[10,14] have pointed out that the valence-band spectra are composed of both bulk- and surface-related features, as far as the 0–5 eV BE window is concerned. Veuillen, Kennou, and Nguyen Tan[10] have shown that the peak located at 1.8 eV below E_F is very sensitive to oxygen exposures, indicating that it is related to a surface state. This is also confirmed by the very narrow width (~300 meV) of the relevant feature as observed on the spectra taken with He_I, Ne_I, and Ne_{II} radiations (Fig. 6). Furthermore, they have found that the

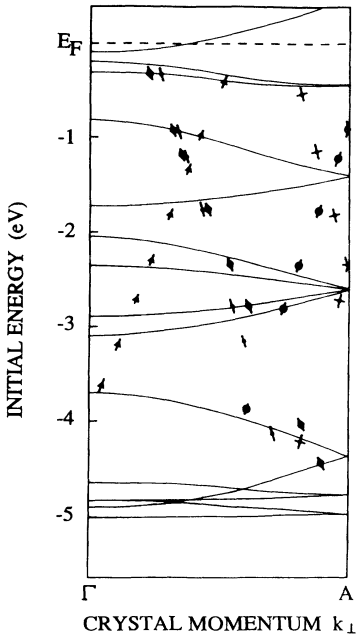

FIG. 7. A comparison between calculated (full lines) band dispersions and experimental data for $ErSi_{1.7}$ as a function of the perpendicular momentum $k_\perp$ along the ΓA direction. The calculations are treated by assuming a $2c$ periodicity along the $ErSi_{1.7}$[0001] axis. The experimental data reported in this figure are those indicated by tics in Fig. 6. Data for He_I, He_{II}, Ne_I, Ne_{II}, and Ar_I photon energies are shown by ϕ, +, $\blacklozenge$, $\blacklozenge$, and $\blacklozenge$ symbols, respectively.

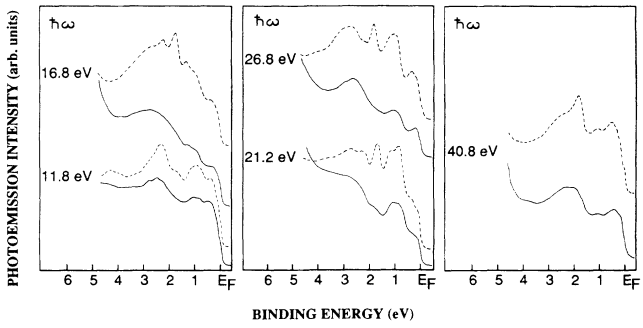

FIG. 8. Normal-emission photoelectron spectra from $ErSi_{1.7}$(0001) before (dashed lines) and after (full lines) exposure to 600 L of O_2 as a function of photon energies.

double structure at 0.9–1.2-eV BE is much less altered by oxygen adsorption, suggesting that it is probably due to bulk transitions. However, no information is available from their experiments about the 2.2-eV BE state.

We have therefore exposed our $ErSi_{1.7}$ surface to 600-L O_2 and then recorded the angle-resolved ultraviolet photoemission spectroscopy (ARUPS) spectra for the five photon energies. Figure 8 displays ARUPS spectra recorded at normal emission before (dashed lines) and after (full lines) exposure to O_2. On the clean $ErSi_{1.7}$ surface, the 2.2-eV BE feature appears as a well-defined peak in the spectra taken with He_I, He_{II}, and Ne_I. On the spectrum taken with Ar_I a rather broad structure is observed at ~2.4-eV BE which probably involves more than one component. Finally, on the spectrum taken with Ne_{II}, one observes only a small shoulder at 2.2 eV. After O_2 exposure, all features of the valence-band spectra are attenuated but it appears that the peaks at 1.8- and 2.2-eV BE are more strongly attenuated than the 0.9–1.2 doublet or the feature near E_F. These results suggest that the structures observed at 1.8- and 2.2-eV BE could arise from surface states, probably superimposed to bulk states. However, a clear determination of the bulk-related states in this BE window remains an open question since exposures to O_2 strongly affect this part of the spectra, leaving only a broad structure centered around 2.5–2.8-eV BE. On the other hand, the small attenuation upon O_2 exposure of the 0.9–1.2-eV features suggests a dominant contribution from bulk states at these energies. A major point here is that as shown in Sec. II B the calculated bands near 1-eV BE are closely related to the presence of Si vacancies. In the absence of vacancies no bulk electronic states are predicted in this spectral region. Thus we attribute the feature at 0.9–1.2-eV BE to electronic states reflecting the defects due to the ordered Si vacancy array. A significant contribution from surface states cannot be ruled out, but the small discrepancies, for both energy location and energy dispersion versus $k_\perp$, between experimental and calculated bands arising from the Si vacancies seem not to be related to the existence of surface states. One may invoke several possible origins of these discrepancies. First, the $ErSi_{1.7}$ crystallographic structure along the c axis used in the calculations is not firmly established. As a matter of fact, we have assumed as a starting point the crystal periodicity along the [0001] axis to be $2c$, c being the

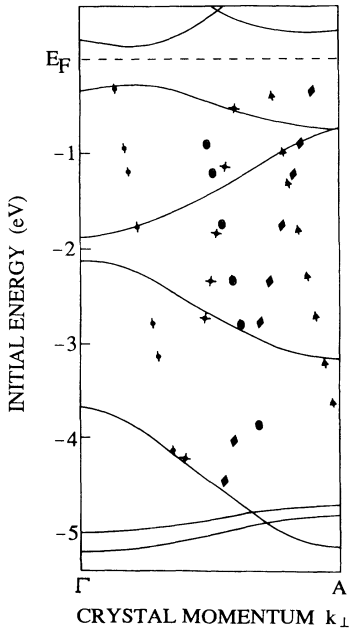

FIG. 9. The same as Fig. 7, but with band dispersions calculated for a c, periodicity along the $ErSi_{1.7}$[0001] axis.

periodicity along this axis of a perfect AlB_2-type crystal. This choice was guided by the experimental evidence of a $2c$ periodicity along the [0001] axis of $YSi_{1.7}$.[9] To see to what extent the bulk band structure is modified by changing the crystal periodicity along c, the bulk band structure has been calculated for a c periodicity. Figure 9 illustrates the calculated bands (full lines) along with experimental data. In contrast with the results displayed in Fig. 7, the fit of the experimental data to the calculated bands becomes very poor. This suggests that the crystal periodicity along the [0001] axis is $2c$ rather than c, as was observed experimentally for the $YSi_{1.7}$ crystal. On an other hand, in the defect AlB_2 model used in the calculations, we have assumed that the Si vacancies are periodically distributed over the silicide without relaxations of Si atoms with respect to their positions in an ideal crystal. So far, we have not made calculations taking into account these Si displacements. However, the two vacancy-related bands labeled (Er $d_{xz,yz}$–Si σ_p) and (Er $d_{x^2-y^2,xy}$–Si σ_p) are twofold degenerated, and one might anticipate that they will split upon changing the Si positions within the Si plane or even perpendicularly to the Si plane. At any rate, the relaxation around the Si vacancies is expected to modify the relevant theoretical bands to an extend compatible with the observed discrepancies.

IV. CONCLUSIONS

A good agreement between experimental and theoretical results is found, despite the presence of surface-related states in the experimental spectra, making their interpretation rather difficult. Thus the experimental measurements in conjunction with theoretical calculations using the extended Hückel method have helped to elucidate the band structure of $ErSi_{1.7}$ silicide permitting, for instance, the identification of the Si-vacancies-related electronic states in the valence-band spectra. Furthermore these results suggest that the $ErSi_{1.7}$ structure periodicity along the [0001] axis is $2c$ rather than c, in agreement with conclusions of Ref. 9 for the $YSi_{1.7}$ system which is isostructural to $ErSi_{1.7}$. However, a precise description of the Si-vacancies-related electronic states needs further investigations, taking into account their possible atomic position relaxation in the $ErSi_{1.7}$ lattice.

ACKNOWLEDGMENTS

The computations have been performed at CCSC (Centre de Calcul de Strasbourg). The authors would like to thank Dr. M. H. Whangbo for a fruitful discussion.

[1]J. A. Knapp and S. T. Picraux, Appl. Phys. **48**, 466 (1986).
[2]J. A. Knapp and S. T. Picraux, in *Thin Films—Interfaces and Phenomena*, edited by R. J. Nemanich, P. S. Ho, and S. S. Lau, MRS Symposia Proceedings No. 54 (Materials Research Society, Pittsburgh, 1986), p. 261.
[3]M. P. Siegal, F. H. Kaatz, W. R. Graham, J. J. Santiago, and J. Van der Spiegel, Appl. Surf. Sci. **38**, 162 (1989).
[4]F. Arnaud d'Avitaya, A. Perio, J. C. Oberlin, Y. Campidelli, and J. A. Chroboczek, Appl. Phys. Lett. **54**, 2198 (1989).
[5]J. Y. Duboz, P. A. Badoz, A. Perio, J. C. Oberlin, F. Arnaud d'Avitaya, Y. Campidelli, and J. A. Chroboczek, Appl. Surf. Sci. **38**, 171 (1989).
[6]P. Wetzel, L. Haderbache, C. Pirri, J. C. Peruchetti, D. Bolmont, and G. Gewinner, Surf. Sci. **251/152**, 799 (1991).
[7]A. Golanski, J. L. Park, S. J. Pennycook, and C. W. White, J. Appl. Phys. **70**, 1853 (1991).
[8]M. Gurvich, A. F. J. Levi, R. T. Tung, and S. Nakahara, Appl. Phys. Lett. **51**, 311 (1987).
[9]R. Baptist, A. Pellissier, and G. Chauvet, Solid State Commun. **68**, 555 (1988); A. Pellissier, thesis, Grenoble, 1989.
[10]J. Y. Veuillen, S. Kennou, and T. A. Nguyen Tan, Solid State Commun. **79**, 795 (1991).
[11]C. Wigren, J. N. Anderson, R. Nyholm, and K. O. Karlson, J. Vac. Sci. Technol. A **9**, 1942 (1991).
[12]W. A. Henle, M. G. Ramsey, F. P. Netzer, R. Cimino, and W. Brown, Solid State Commun. **71**, 657 (1983).
[13]S. Gokale, S. Mahamuni, S. V. Deschukh, V. J. Rao, A. S. Nigavekar, and S. K. Kulkarni, Surf. Sci. **237**, 127 (1990).
[14]P. Paki, U. Kafader, P. Wetzel, C. Pirri, J. C. Peruchetti, D. Bolmont, and G. Gewinner, Surf. Sci. **269/270**, 970 (1992).
[15]J. Y. Veuillen, L. Magaud, D. B. B. Lollman, and T. A. Nguyen Tan, Surf. Sci. **269/270**, 964 (1992).
[16]R. Hoffmann, J. Chem. Phys. **39**, 1399 (1963).
[17]M. H. Wangbo and R. Hoffmann, J. Am. Chem. Soc. **100**, 6093 (1978); C. Minot, M. A. Van Hove, and G. A. Somorjai, Surf. Sci. **127**, 441 (1983).
[18]R. Hoffmann and P. Hofmann, J. Am. Chem. Soc. **98**, 598 (1976); J. H. Ammeter, H. B. Brügi, J. Thibeault, and R. Hoffmann, *ibid.* **100**, 3686 (1976).
[19]C. Minot and L. Stauffer (unpublished).